Chemistry–A European Journal
Research Article
doi.org/10.1002/chem.202401331
Chemistry Europe
European Chemical Societies Publishing
www.chemeurj.org

# Polymeric Nanozyme with SOD Activity Capable of Inhibiting Self- and Metal-Induced α-Synuclein Aggregation

Álvaro Martínez-Camarena,*[a, b, c, d] Francesco Bellia,[e] M. Paz Clares,[a] Graziella Vecchio,[c] Julien Nicolas,*[b] and Enrique García-España*[a]

Despite decades of research, Parkinson's disease is still an idiopathic pathology for which no cure has yet been found. This is partly explained by the multifactorial character of most neurodegenerative syndromes, whose generation involves multiple pathogenic factors. In Parkinson's disease, two of the most important ones are the aggregation of α-synuclein and oxidative stress. In this work, we address both issues by synthesizing a multifunctional nanozyme based on grafting a pyridinophane ligand that can strongly coordinate $Cu^{II}$, onto biodegradable PEGylated polyester nanoparticles. The resulting nanozyme exhibits remarkable superoxide dismutase activity together with the ability to inhibit the self-induced aggregation of α-synuclein into amyloid-type fibrils. Furthermore, the combination of the chelator and the polymer produces a cooperative effect whereby the resulting nanozyme can also halve $Cu^{II}$-induced α-synuclein aggregation.

## Introduction

Neurodegenerative diseases are one of the major health challenges that modern societies face nowadays, with Parkinson's disease (PD) being one of the most ubiquitous ones. According to the World Health Organization, PD affected nearly 8.5 million individuals in 2019, 329 000 of whom perished from this illness.[1] The tendency seems to be towards worsening the situation impelled by factors such as the increasing population ageing.[2] The prevalence of PD has indeed doubled since 1990,[3,4] while both disability and mortality resulting from PD are increasing faster than from any other neurological disorder, including Alzheimer's disease.[1,4,5]

From a pathological point of view, PD is a debilitating neurodegenerative disorder characterized by the progressive degeneration of dopaminergic neurons in the substantia nigra, leading to a range of motor symptoms (shaking of extremities, rigidity, limited mobility) and non-motor complications (neurological and psychiatric issue, sleep-wake disorders, depression, pain and sensory disturbances such as anosmia).[2,6] Despite decades of research, PD is still an idiopathic disease for which no cure has yet been found.[2,6,7] Notwithstanding this, multiple studies have suggested that oxidative stress and peptide aggregation may play important roles in the generation and progression of PD.[5,8–12]

Oxidative stress can be defined as the imbalance between the production of reactive oxygen species (ROS) and the ability of the endogenous antioxidant systems of the organism to scavenge them.[5,8] Thus, the pathogenic character of these species does not lie in ROS themselves, but in their accumulation, which can lead to oxidative damage to lipids, proteins, DNA and RNA.[5] On the other hand, peptide aggregation is a complex process in which normally soluble proteins (mainly intrinsically disordered proteins, IDPs) misfold and aggregate into insoluble, toxic structures such as amyloid fibrils.[13,14] In PD, aggregation of α-synuclein (Syn) leads to the formation of Lewy bodies.[12]

A subjacent factor in both oxidative stress and peptide aggregation is the misregulation of redox-active first-row transition metals such as $Cu^{II}$ and $Fe^{II}$. On the one hand, these metal ions can be coordinated by the monodisperse peptides thus prompting its aggregation and, on the other hand, the resulting systems can work as ROS sources due to the Fenton and Haber–Weiss chemistry of the resulting metal complexes.[15,16] Moreover, oxidative stress can also result in protein misfolding and aggregation, accelerating the degeneration process.[9–11] Thus, it is clear that oxidative stress and peptide aggregation are interrelated events in the pathogenesis of PD. Consequently, some of the strategies currently being pursued to address the emergence of PD rely on the development of antioxidant systems able to prevent the accumulation of ROS or to inhibit the formation of α-synuclein aggregates.[14]

[a] Á. Martínez-Camarena, M. Paz Clares, E. García-España
ICMol, Departament de Química Inorgànica, Universitat de València, C/ Catedrático José Beltrán 2, Paterna 46980, Spain
E-mail: alvaro45@uv.es
enrique.garcia-es@uv.es
[b] Á. Martínez-Camarena, J. Nicolas
Institut Galien Paris-Saclay, CNRS, Université Paris-Saclay, Orsay 91400, France
E-mail: julien.nicolas@universite-paris-saclay.fr
alvaro45@uv.es
[c] Á. Martínez-Camarena, G. Vecchio
Dipartimento di Scienze Chimiche, Università degli Studi di Catania, Viale A. Doria 6, Catania 95125, Italy
[d] Á. Martínez-Camarena
MatMoPol Research Group, Departamento de Química Inorgánica, Facultad de Ciencias Químicas, Universidad Complutense de Madrid, Avda. Complutense s/n, Madrid 28040, Spain
[e] F. Bellia
Istituto di Cristallografia, CNR, P. Gaifami 18, Catania 95126, Italy

Supporting information for this article is available on the WWW under https://doi.org/10.1002/chem.202401331

Considering the major role of superoxide radicals in ROS generation,[17] research on antioxidant systems has centered on the development of small ionophores whose $Cu^{II}$,[18–25] $Fe^{II}$,[18] $Mn^{II}$,[18,26,27] and $Zn^{II}$[28] complexes present superoxide dismutase (SOD) activity. Although very few such systems have yet displayed satisfactory clinical results,[29,30] the use of tetraazamacrocycles and nanotechnology are two of the emerging promising approaches to tackle neurodegenerative diseases involving oxidative stress.[20–24,31–34] In this context, we have recently observed that the modification of non-toxic boehmite nanoparticles (BNPs) with binuclear $Cu^{II}$ azamacrocycles can significantly enhance the SOD activity of such complexes.[25,31,33,35] But there is little point in eliminating ROS without disrupting the source that generates them, which are the α-synuclein peptide aggregates in the case of PD. To our knowledge, although various approaches aimed at inhibiting the formation of peptide aggregates have been studied so far,[36–39] very few of them have shown satisfactory, dual inhibitory/antioxidant activity.[14,40–42] One reason for this is that these two pathogenic aspects of PD have largely been treated as separate events, with research generally based on the development of systems only focusing on one of them. This is partly due to the difficulty of generating systems with sufficiently high dual activity (antioxidant and aggregation inhibitory) without interfering between the two.

To overcome this handicap, we developed a dual activity nanoscale system capable of both removing reactive oxygen species and inhibiting the formation of α-synuclein aggregates as sources of ROS. In other words, we set out to create a multitasking therapeutic tool that moves from the "one-molecule, one-target" paradigm to the "one-molecule, one-disease" one. The novel approach we present is based on the design of a multifunctional nanozyme composed of biocompatible and biodegradable polymer nanoparticles (NPs) functionalized with a well-known SOD mimic (Figure 1)[43] The designed NPs are based on poly(lactic acid)-*block*-poly(ethylene glycol) (PLA-*b*-$PEG_{5k}$-$CH_2COOH$) diblock copolymers, in which the PLA block constitutes the hydrophobic core of the NPs, while the hydrophilic PEG block forms the shell.[44] The COOH end-group of the PEG block enables the conjugation with the SOD mimic, resulting in NPs with surface-exposed SOD units, forming the so-called nanozymes. The PLA-*b*-$PEG_{5k}$-$CH_2COOH$ NPs were chosen due to their biocompatibility, biodegradability, low toxicity and high colloidal stability in water, as well as to their proven capacity to interact with peptides and IDPs such as amyloid-beta ($A\beta_{1-42}$).[44–46] 5-(2-Aminoethyl)-2,5,8-triaza[9]-2,6-pyridinophane (**L**)[47] was selected as SOD mimic due to the proven antioxidant activity of its $Cu^{II}$ complexes, as well as the potential lack of detrimental effect of its coupling to the copolymer on the $Cu^{II}$ coordination mode. Grafting the SOD mimic onto the copolymer not only aims to combine the antioxidant and the antiaggregant activities into a single nanoscale system, but also to boost the SOD activity of the $Cu^{II}$-**L** complex, as previously observed with similar ligands.[31,33] In order to evaluate the influence of **L** density on the surface of the nanoparticles, the nanozymes were prepared with different **L** payloads. Thus, the antioxidant and Syn aggregation inhibitory activity of the nanozymes was evaluated as a function of the concentration of **L** on their surface.

## Results and Discussion

### Synthesis of 5-(2-Aminoethyl)-2,5,8-Triaza[9]-2,6-Pyridinophane·3HBr (L·3HBr)

5-(2-Aminoethyl)-2,5,8-triaza[9]-2,6-pyridinophane·4HBr (L·4HBr) was synthesized following a modification of the Richman-Atkins procedure, followed by subsequent detosylation using HBr/HAc in the presence of phenol.[47] The obtained hydrobromide salt of the compound was characterized by NMR and elemental microanalysis (see Figure S1). The NMR spectrum indicated the desired structure. In particular, the triplet and the doublet located at 8.06 and 7.57 ppm, respectively, are characteristic of the ε and ζ protons of the pyridine moiety. The singlet of the benzylic protons (η) is located at 4.30 ppm, partially overlapping with the proton signal from $H_2O$ used as a solvent. Finally, a series of three multiplets characteristic of the aliphatic hydrogens can be observed between 3.5 and 2.9 ppm, which are associated with the θ, ι, κ and μ hydrogens of L. On the other hand, elemental microanalysis revealed percentages of C, H and N compatible with the tetraprotonated (L·4HBr) form of L.

### Synthesis of PLA-*b*-$PEG_{5k}$-$CH_2COOH$

The PLA-*b*-$PEG_{5k}$-$CH_2COOH$ diblock copolymer was synthesized by ring-opening polymerization of D,L-lactide in presence of HO-$PEG_{5k}$-$CH_2COOH$ as the initiator, and was characterized by $^1$H-NMR and SEC (Figures S2–S4 in ESI).[45] The $^1$H-NMR spectrum (Figures S2 and

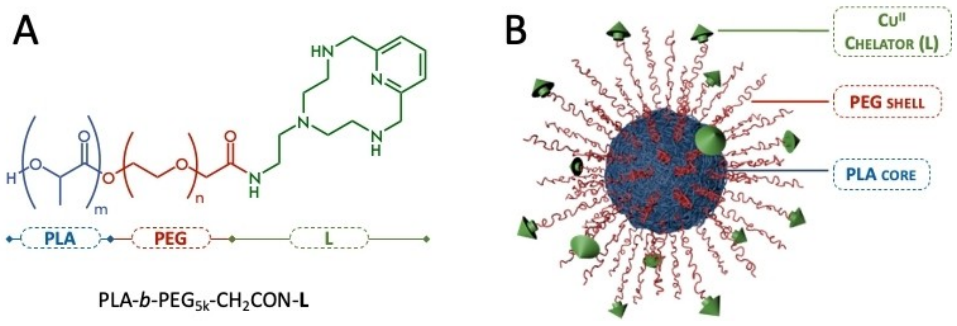


**Figure 1.** (A) Structure of the PLA-*b*-$PEG_{5k}$-$CH_2CON$–L polymer and (B) representation of the nanozymes based on polymeric nanoparticl.

S4A) proved the fulfilment of the copolymerization, which is confirmed by the presence of the PLA protons at 1.60 (3 H) and 5.2 (1 H) ppm. Integrations of the η signal (2 H) of D,L-lactide at 5.0–5.1 ppm and the β signal (2 H) of PLA at 5.1–5.2 ppm (see Figure S2 in ESI) allowed us to determine a conversion of 95%. Successful purification was evidenced by the absence of D,L-lactide proton signals η and ϕ (see Figure S3 in ESI). The $M_n$ of PLA-*b*-PEG$_{5k}$-CH$_2$COOH diblock copolymer was calculated by comparing the peak area of the α protons of the PEG block with that corresponding to the β protons of the PLA block, giving $M_n = 26\,850\ g\,mol^{-1}$. Dispersity ($Đ$) was measured by SEC in $CHCl_3$ and gave $M_w/M_n = 1.50$ (Figure S4B). Interestingly, no signal is observed on the SEC chromatogram under UV detection (Figure S4B), which allows us to consider the detection of the ligand after coupling to the copolymer.

### Synthesis of PLA-*b*-PEG$_{5k}$-CH$_2$CON-L

Conjugation of **L** to PLA-*b*-PEG$_{5k}$-CH$_2$COOH was carried out by Steglich esterification and was assessed by $^1$H-NMR and SEC. The analysis of the $^1$H-NMR spectrum of the purified copolymer revealed the presence of **L**, suggested by the aliphatic θ signals and the characteristic ε and ζ peaks of the pyridine moiety at 7.75 and 7.22 ppm, respectively (Figure 2). Nevertheless, direct evaluation of the covalent linkage with the terminal carboxylic acid group of the PEG block was not possible because of the overlay of many signals in the characteristic region of the NMR spectrum.

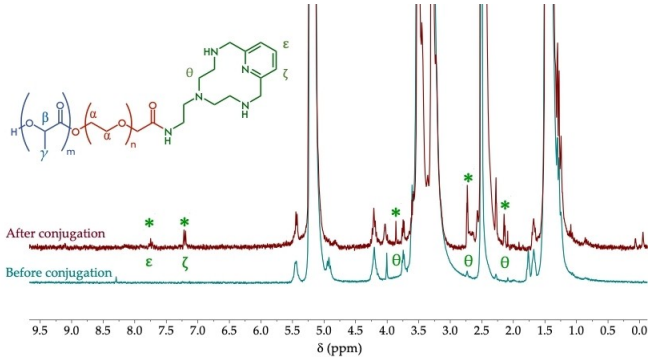


**Figure 2.** $^1$H-NMR spectra in DMSO-$d_6$ of the purified PLA-*b*-PEG$_{5k}$-CH$_2$COOH diblock copolymer before (green) and after (red) conjugation of **L**.

Successful coupling of **L** to PLA-*b*-PEG$_{5k}$-CH$_2$COOH was confirmed by SEC, which exhibited a strong UV absorbance at 260 nm (to follow the pyridine absorbance band) that overlapped perfectly with the RI trace of the copolymer (Figure 3A). This suggested a homogeneous coupling of **L** on the entire molar mass distribution of the copolymer. In contrast, the non-functionalized PLA-*b*-PEG$_{5k}$-CH$_2$COOH copolymer showed no UV signal (Figure 3B). It is also important to note that coupling of **L** to the copolymer (and the purification of the resulting conjugate) did not lead to significant modification of its macromolecular characteristics, since the RI chromatograms for both PLA-*b*-PEG$_{5k}$-CH$_2$COOH and PLA-*b*-PEG$_{5k}$-CH$_2$CON-**L** were nearly perfectly overlaid (Figure 3C). From SEC, the PLA-*b*-PEG$_{5k}$-CH$_2$CON-**L** exhibited a dispersity of 1.68.

Purification of PLA-*b*-PEG$_{5k}$-CH$_2$CON-**L** removed all unreacted **L**. As shown in Figure S5, SEC performed in DMSO (since **L** is not soluble in $CHCl_3$) of a physical mixture of PLA-*b*-PEG$_{5k}$-CH$_2$CON-**L** and free **L** (1 eq) showed sharp peaks at 12.7–12.8 min on the RI and UV chromatograms (in DMSO), which correspond to free **L**. However, these peaks were not present on the SEC chromatograms of PLA-*b*-PEG$_{5k}$-CH$_2$CON-**L** alone. This suggests that all the observed **L** in the $^1$H-NMR spectrum of PLA-*b*-PEG$_{5k}$-CH$_2$CON-**L** was conjugated to the copolymer.

### Formulation of L-Functionalized Nanoparticles

NPs with different surface densities in **L** were obtained by conanoprecipitation[45,48] of PLA-COOMe and a mixture of PLA-*b*-PEG$_{5k}$-CH$_2$CON-**L**/PLA-*b*-PEG$_{5k}$-CH$_2$COOH (with a weight fraction of PLA-*b*-PEG$_{5k}$-CH$_2$CON-**L** ranging from 0 to 60 wt.% in the copolymer content).

At an overall concentration of $10\ mg\,mL^{-1}$ in water, the resulting NPs exhibited mean diameters in the ~130–230 nm

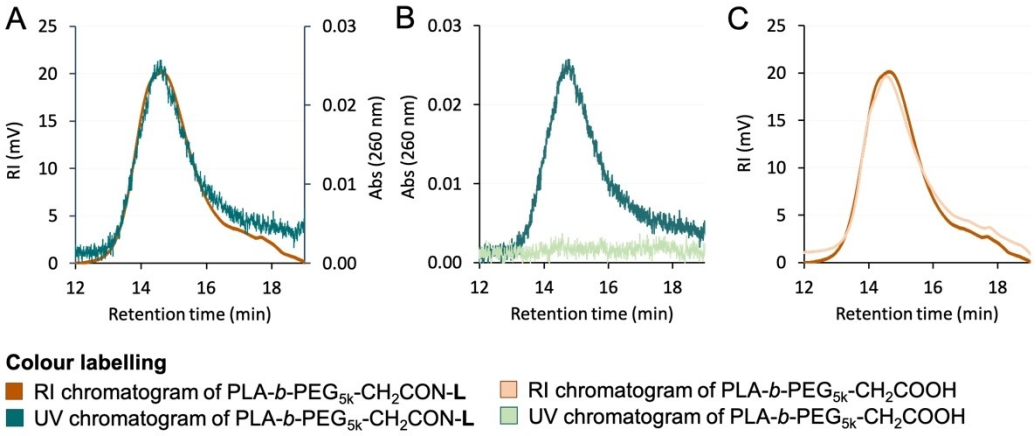


**Figure 3.** (A) SEC chromatograms of PLA-*b*-PEG$_{5k}$-CH$_2$CON-**L** under RI (orange) and UV (green) detections. (B) Comparison of the UV signal of the chromatograms of PLA-*b*-PEG$_{5k}$-CH$_2$CON-**L** (dark green) and PLA-*b*-PEG$_{5k}$-CH$_2$COOH (pale green). (C) Comparison of the RI signal of the chromatograms of PLA-*b*-PEG$_{5k}$-CH$_2$CON-**L** (dark orange) and PLA-*b*-PEG$_{5k}$-CH$_2$COOH (pale orange). All the SEC analyses were performed in $CDCl_3$. The UV was recorded at 260 nm in all the cases.

**Table 1.** Intensity-average diameters ($D_z$), polydispersity indexes (PDI) and ζ-potentials of the nanoparticles after nanoprecipitation as a function of the PLA-*b*-$PEG_{5k}$-$CH_2CON$-**L** weight fraction in the copolymers and of the presence of Cu (1 : 1 $Cu^{II}$:L).

| Amount of PLA-*b*-$PEG_{5k}$-$CH_2CON$–L in the copolymer fraction (wt.%) | Dz ± SD (mV) | | PDI ± SD (mV) | | ζ-pot ± SD (mV) | |
|---|---|---|---|---|---|---|
| | without $Cu^{II}$ | with $Cu^{II}$ | without $Cu^{II}$ | with $Cu^{II}$ | without $Cu^{II}$ | with $Cu^{II}$ |
| 0 | 151 ± 1 | – | 0.13 ± 0.01 | – | −34 ± 1 | – |
| 20 | 127 ± 7 | 127 ± 4 | 0.10 ± 0.02 | 0.13 ± 0.03 | −32.0 ± 0.9 | −29.5 ± 0.8 |
| 40 | 176 ± 4 | 169 ± 3 | 0.34 ± 0.07 | 0.31 ± 0.03 | −31.5 ± 0.2 | −28 ± 1 |
| 50 | 232 ± 5 | 223 ± 1 | 0.28 ± 0.03 | 0.29 ± 0.03 | −30.6 ± 0.4 | −28.6 ± 0.4 |
| 60 | 960 ± 60 | 870 ± 30 | 0.14 ± 0.07 | 0.22 ± 0.07 | −27.1 ± 0.2 | −30.9 ± 0.7 |

range, with relatively narrow particle size distributions (Table 1, Figures 4 and 5), except for the formulation containing 60 wt.% of the conjugated copolymer, that formed particles of *ca.* 800 nm in diameter. ζ-potential measurement of the NPs led to strongly negative surface charge values ranging from −34 mV for the NPs with 0 wt.% of **L**-containing copolymer, to −27 mV for those with 60 wt.% (Table 1 and Figure S6). The decrease, in absolute value, of the surface charge with the increase of the amount of PLA-*b*-$PEG_{5k}$-$CH_2CON$-**L** in the formulation can be explained by the lower amount of carboxylic acid groups (*i.e.*, negative charges) and the higher amount of protonated amino groups from **L** (*i.e.*, positive charges) exposed at the NP surface. All NPs up to 50 wt.% of PLA-*b*-$PEG_{5k}$-$CH_2CON$-**L** exhibited excellent colloidal stability upon storage for at least 27 days, as shown by the constant average diameters with time (Figure 5).

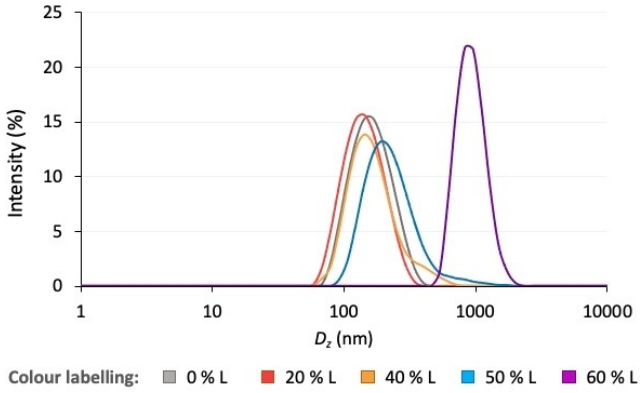


**Figure 4.** Dynamic light scattering (DLS) data showing the intensity-distribution size of the NPs at 25 °C after 27 days, as a function of the PLA-*b*-$PEG_{5k}$-$CH_2CON$-**L** content in the copolymer mixture.

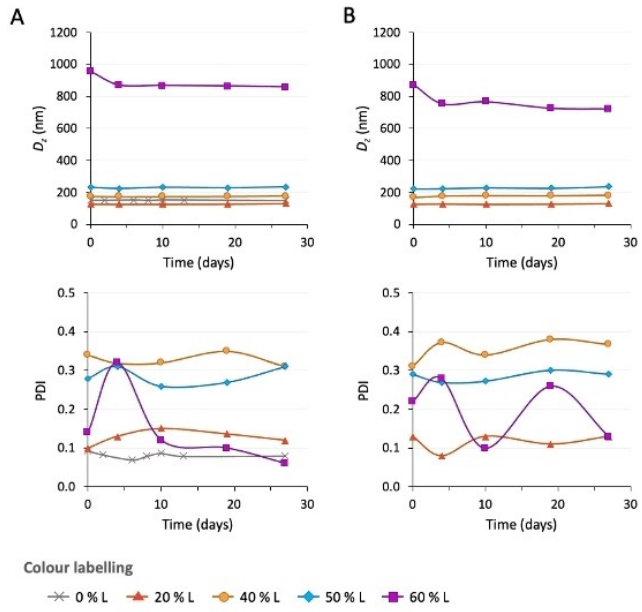


**Figure 5.** Evolution of the intensity-average diameters (Dz) and polydispersity indexes (PDI) of the NPs at 25 °C, (A) in the absence and (B) in presence of $Cu^{II}$ (1 : 1 $Cu^{II}$:L) in solution.

The NPs were then evaluated for their capacity to coordinate $Cu^{II}$. For this, an excess of $Cu^{II}$ (final concentration of 2.5 μM) was added to a solution containing the NPs ([L] ranging from 0 to 1.7 μM) at pH 5. After centrifugation (20 min, 6000 rpm, 4 °C), the supernatant was analyzed by ICP-MS, thus determining the non-coordinated $Cu^{II}$ and, by subtraction, the amount of $Cu^{II}$ coordinated to the NPs. The results are shown in Table 2.

The results indicated that the **L**-functionalized NPs were able to coordinate $Cu^{II}$ in an almost quantitative manner and mainly through a $Cu^{II}$-**L** interaction, since [$Cu^{II}$] coordinated to the NPs is almost identical to the $[\mathbf{L}]_{NPs}$. The carboxylic groups from PLA-*b*-$PEG_{5k}$-$CH_2COOH$ were only barely able to chelate $Cu^{II}$ as evidenced by the low concentration of coordinated $Cu^{II}$ for NPs containing no PLA-*b*-$PEG_{5k}$-$CH_2CON$-**L** copolymer (Table 2, entry 1). When the amount of PLA-*b*-$PEG_{5k}$-$CH_2CON$-**L** is 60 wt.% (Table 2, entry 5), the NPs coordinated a substantially smaller amount of $Cu^{II}$ than theoretically predicted (0.92 *vs*

**Table 2.** Theoretical and experimental concentrations of $Cu^{II}$ coordinated to the NPs determined in Milli-Q water at pH 5, as a function of the amount of PLA-*b*-$PEG_{5k}$-$CH_2CON$-**L** in the copolymer fraction.

| Amount of PLA-*b*-$PEG_{5k}$-$CH_2CON$–L in the copolymer fraction (wt.%) | Concentration of $Cu^{II}$ coordinated to NPs ± SD (μM) | |
|---|---|---|
| | Theoretical | Experimental |
| 0 | 0 | 0.28 ± 0.06 |
| 20 | 0.57 | 0.52 ± 0.05 |
| 40 | 1.13 | 1.13 ± 0.03 |
| 50 | 1.41 | 1.49 ± 0.02 |
| 60 | 1.70 | 0.92 ± 0.05 |

1.70 μM). This could be explained by: (i) aggregation of NPs into bigger size aggregates and/or (ii) interactions between surface exposed **L** because of their high surface density, which would in both cases reduce the number of available surface-exposed **L** receptors and thus the coordination capacity of the NPs. Therefore, NPs with a fraction of PLA-*b*-$PEG_{5k}$-$CH_2CON$-**L** among the copolymer content ranging from 20 to 50 wt.% represented a good compromise as they showed a good correlation between experimental $Cu^{II}$ concentrations and the theoretical calculations.

The presence of $Cu^{II}$ ($Cu^{II}$:**L**; 1:1) in solution did not significantly modify the colloidal characteristics nor the stability of the NPs, although it led to a slight decrease in their ζ-potential (Table 1, Figure S6). This can be explained by the coordination of $Cu^{II}$ to **L**, which would increase the number of positive charges on the surface of the NPs. The opposite trend was observed with the NPs containing the highest amount of **L**-containing copolymer, but this result should be taken with caution due to the unstable and heterogeneous NP suspension.

### Superoxide Dismutase Activity

The capacity of the different nanozymes to catalyze the dismutation of the superoxide anions (abbreviated as SOD activity) was determined through the McCord-Fridovich method. The xanthine/xanthine oxidase system was employed as a source of superoxide radicals, while the reduction of nitro blue tetrazolium salt to blue formazan was used to determine the $O_2^{\cdot-}$ generation rate. The NBT reduction was progressively inhibited after the addition of the solutions with increasing concentrations of the complex. The percentage of inhibition of the NBT reduction was used as a measure of the SOD activity of the compounds. This method allowed us to calculate the $IC_{50}$ and $k_{cat}$ (catalytic constant) values of the SOD mimics. The results of the studies are shown in Figure 6, while the $IC_{50}$ and $k_{cat}$ values can be found in Table 3.

Several conclusions can be drawn from the analysis of the SOD activity results. Firstly, NPs containing **L**-functionalized copolymers coordinated with $Cu^{II}$ (the so-called nanozymes) showed a significant SOD activity. Indeed, the $k_{cat}$ values determined for the **L**-functionalized NPs rank at the upper part of the range when compared with other $Cu^{II}$ and $Mn^{II}$ complexes of small ligands and nanostructured systems, whose $k_{cat}$ typically takes values from $0.5\times10^6$ to $60\times10^6$ $M^{-1}s^{-1}$.[21,22,24,51] However, when **L** is not present on the surface of the NPs, they were not able to coordinate $Cu^{II}$, which resulted in no SOD activity, as shown during the blank experiments. Similarly, the presence of **L** onto the NPs in the absence of $Cu^{II}$ did not lead to a removal of superoxide radicals, as expected (Figure S8).

Secondly, conjugation of **L** to the copolymer did not reduce the $k_{cat}$ value of the $Cu^{II}$ complexes, which ranges between $2.1\times10^6$ and $2.7\times10^7$ $M^{-1}s^{-1}$, both for the complex free in solution and grafted onto the copolymer. This suggests a minimal influence of **L** conjugation to the copolymer on the coordination mode of $Cu^{II}$ by **L**. Thirdly, increasing the amount of PLA-*b*-$PEG_{5k}$-$CH_2CON$-**L** resulted in up to a 13-fold increase in

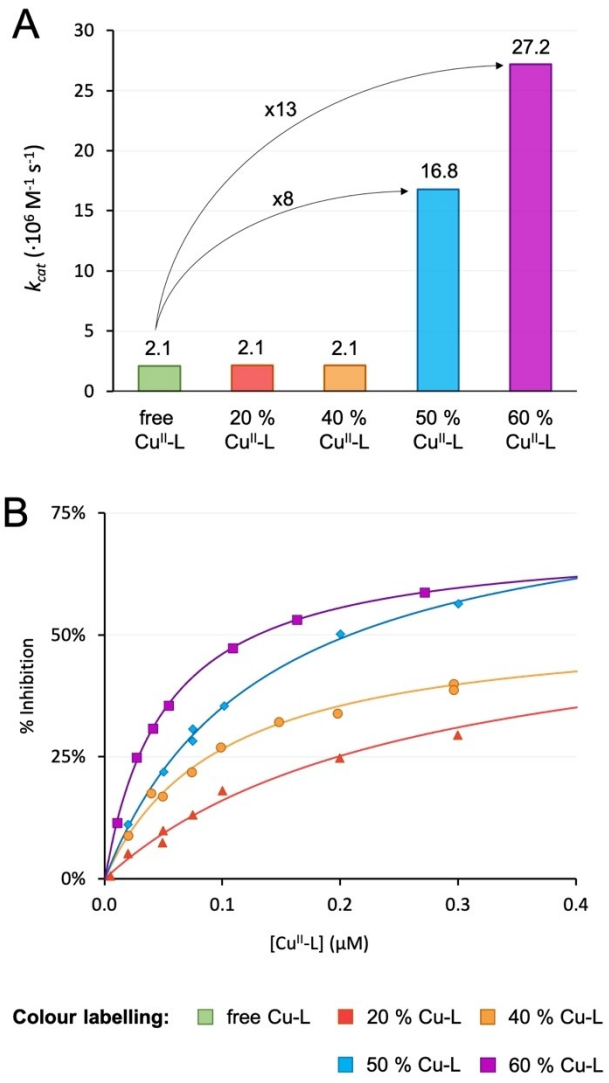


**Figure 6.** (A) Evolution of the $k_{cat}$ values of the $Cu^{II}$:PLA-*b*-$PEG_{5k}$-$CH_2CON$-**L** complexes as a function of the amount of PLA-*b*-$PEG_{5k}$-$CH_2CON$-**L** in the copolymer content in the NPs. (B) Fittings of the SOD activity data obtained by the McCord-Fridovich method for the NPs as a function of the concentration of the amount of PLA-*b*-$PEG_{5k}$-$CH_2CON$-**L** in the copolymer content.

**Table 3.** Evaluation of the SOD activity of the PLA-*b*-$PEG_{5k}$-$CH_2CON$-**L** NPs when coordinating $Cu^{II}$ at pH 7.4.

| Compound | $IC_{50}\pm$SD (μM) | $k_{cat}$ ($10^6$ $M^{-1}$ $s^{-1}$) |
|---|---|---|
| **L**[a] | 1.42 | 2.1 |
| PLA-*b*-$PEG_{5k}$-$CH_2CON$-**L** 20% | 1.6 ± 0.5 | 2.1 |
| PLA-*b*-$PEG_{5k}$-$CH_2CON$-**L** 40% | 1.6 ± 0.5 | 2.1 |
| PLA-*b*-$PEG_{5k}$-$CH_2CON$-**L** 50% | 0.21 ± 0.02 | 16.8 |
| PLA-*b*-$PEG_{5k}$-$CH_2CON$-**L** 60% | 0.130 ± 0.004 | 27.2 |
| $Cu(ClO_4)_2$[b] | 1.1 ± 0.1 | 2.7 |
| CuZn-SOD[b] | 0.010 ± 0.002 | 430 |

[a] Values taken from ref. [49]. [b] Values taken from ref. [50].

the $k_{cat}$ values of the complexes. This could be due to the less negative ζ-potential values of the NPs containing the highest surface densities of **L**, which would reduce the electrostatic repulsion between the superoxide substrate and the NPs, as previously observed with other nanostructured systems based on boehmite and silica nanoparticles grafted with similar $Cu^{II}$-polyamine complexes.[21,31,33]

### Antiaggregant Activity Towards Self- and Metal-Induced Aggregation Assay of α-Synuclein

The pathological route of PD involves, among many other biochemical events, the amyloid-type aggregation of Syn. This protein, like other IDPs, for reasons as still unknown, undergoes a significant misfolding that makes the protein more prone to form soluble and toxic oligomers, then larger aggregates and amyloid fibrils that, in turn, are stored in the cerebral areas.[12–14] Importantly, such a process is accelerated by metal ions like $Cu^{II}$.[52] Inhibiting the aggregation process of Syn is one of the main goals to mitigate or prevent the onset of PD. Therefore, the capacity of the nanozymes to hinder the *in vitro* self- and metal-induced aggregation of Syn was tested.

All the NPs containing 0 to 50 wt.% of PLA-*b*-$PEG_{5k}$-$CH_2CON$-**L** were considered for these assays, discarding those with 60 wt.% due to their tendency to precipitate. The aggregation of Syn into amyloid-like fibrils was followed using thioflavin T (ThT), a fluorescent dye capable of selectively recognizing amyloid fibrils.[53,54] Upon binding, ThT exhibits a drastic increase in fluorescence, allowing the kinetics of formation of the amyloid-like Syn aggregates to be studied in real time (see Figure S9).[54] The capacity of the studied nanozymes to inhibit the formation of the Syn aggregates was calculated as the difference between the fluorescence of the solution at time 0 and the maximum absorbance reached ($F_{max}$–$F_0$), and was represented as aggregation extent % (Figure 7). Since $F_{max}$–$F_0$ is proportional to the amount of Syn fibrils, the lower $F_{max}$–$F_0$ is, the better the antiaggregant activity.[55] Control experiments with Syn alone or co-incubated with **L** were also carried out.

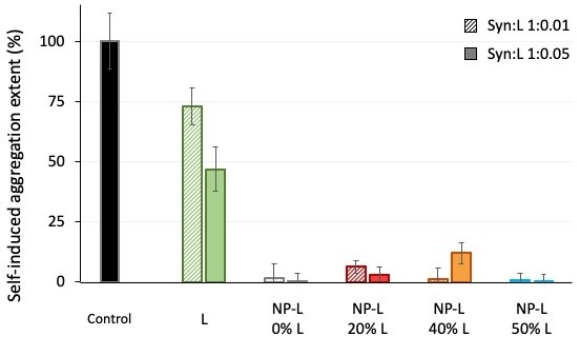


**Figure 7.** Relative self-induced aggregation extent of Syn alone (control) or co-incubated with L or NPs containing different amounts of PLA-*b*-$PEG_{5k}$-$CH_2CON$-**L** in the copolymer fraction (0 to 50%).

The main observation that can be drawn from the results is that, under the used conditions, the nanozymes are able to almost completely inhibit Syn aggregation into amyloid-type aggregates. Regardless of the **L** loading on the NPs and the Syn:L ratio used, the fluorescence due to the ThT-sensitive amyloid species was almost zeroed in the presence of all the nanozymes. Moreover, free **L** in solution is only capable of partially inhibiting the aggregation of Syn. This clearly points out that the polymer itself somehow interacts with the Syn, preventing the formation of amyloid-type species. This is in line with previous studies involving amyloid-beta peptides instead of Syn, in which it was observed that the PEG chains are capable of binding the peptide.[45]

Except for free **L**, the inhibition of aggregation by nanozymes does not seem to depend on the Syn:L ratio (0.01 and 0.05). In an attempt to differentiate the antiaggregant effect of the copolymers as a function of the loading level in **L** of the nanozymes, as well as to analyze the effect of a smaller ratio in such activity, the nanozymes with 0 and 50% loading levels of **L** were evaluated using an even lower Syn:L molar ratio (1:0.001). The fluorescence gain ($F_{max}$–$F_0$) and the time needed to reach lag phase ($t_{lag}$) are listed in Table 4. As an indication, the lower $F_{max}$–$F_0$ is and/or the higher $t_{lag}$ is, the better the antiaggregant activity.[55]

Clear differences between **L** loading levels can be observed when Syn:L ratio is reduced to 1:0.001. Under these conditions, an increase in the **L** loading of the nanozymes has a positive effect on the inhibition of the Syn aggregation. NPs with a higher surface density in **L** lead to smaller fluorescence gains (less Syn aggregated) and longer lag phase times, to the extent that the variation in fluorescence is not detectable for NPs containing 50% PLA-*b*-$PEG_{5k}$-$CH_2CON$-**L** in the copolymer fraction. Moreover, the maximum fluorescence gain reached by Syn alone (*control*) slightly differs from that reported in the presence of **L**, while **L**-free NPs induce an even greater fluorescence gain than the one shown by Syn alone. The trend of the $t_{lag}$ values is in line with these results. These observations clearly state that not only the copolymer but also the **L** grafted onto the NPs have a key role in hindering Syn self-aggregation into amyloid-type fibrils.

**Table 4.** Kinetic parameters related to the self-induced aggregation of Syn alone (control) or co-incubated with **L** or NPs containing different amounts of PLA-*b*-$PEG_{5k}$-$CH_2CON$-**L** in the copolymer fraction (0 to 50%). The Syn:L molar ratio was 0.001.

| | Control | L | NP–L 0% | NP–L 20% | NP–L 40% | NP–L 50% |
|---|---|---|---|---|---|---|
| $F_{max}$–$F_0$ ($\times 10^5$) | 2.47 ± 0,06 | 2.34 ± 0.05 | 3.47 ± 0.09 | 2.75 ± 0.08 | 2.00 ± 0.08 | – |
| $t_{lag}$ (h) | 117 ± 4 | 123 ± 3 | 100 ± 2 | 131 ± 1 | 134 ± 1 | > 160 |

[a] $p < 0.001$ vs Control. [b] $p < 0.05$ vs Control; One-Way ANOVA followed by t-test.

Finally, the **L**-loaded nanozymes seem also to partially inhibit metal-induced Syn aggregation. Indeed, NPs with 50% loading levels in **L** reduce by half the aggregation extent of the Syn in the presence of $Cu^{II}$ (see Figure 8). Moreover, the presence of **L** seems to be required to inhibit the metal-induced aggregation of Syn since 0% **L**-loaded NPs do not show any antiaggregant activity. This result is consistent with previous ICP-MS measurements, which indicated that NPs containing 0% of **L** lacked the ability to capture $Cu^{II}$ in solution efficiently. Finally, free **L** presents similar activities to those shown by the 50% **L**-loaded NPs, *i.e.* the loading of **L** onto the NPs preserves the activity of the first as an inhibitor of metal-induced Syn aggregation. This could be an important element for future work since NPs functionalized with **L** have more chance to work in vivo conversely to free **L**, which could present higher diffusion through the organism and a faster degradation, among other issues.

These results are remarkable since metal-induced (particularly $Cu^{II}$-induced) aggregation is a key mechanism to consider as it is faster than the self-induced one. Therefore, the fact that the developed nanozymes have the ability to hinder Syn aggregation even in the presence of $Cu^{II}$ by altering the levels of this metal in solution may represent an important step forward in the development of new medicines for PD.

## Conclusions

In this article, we proved that combining a pyridinophane-type ligand with polymer NPs is a promising strategy for designing multifunctional nanozymes. On the one hand, the pyridinophane ligand can capture free $Cu^{II}$ in solution giving rise to complexes with SOD activity and, consequently, being able to reduce oxidative stress. On the other hand, the nanozymes resulting from grafting the pyridinophane ligand on the PLA-*b*-$PEG_{5k}$-$CH_2COOH$ NPs are able to reduce self-induced Syn aggregation in a semi-quantitative manner in the absence of $Cu^{II}$. More importantly, the combination of the chelator with the copolymer generates a cooperative system in which the nanozymes are upgraded with the ability to capture $Cu^{II}$, enabling them not only to catalyze the dismutation of superoxide anions, but also to inhibit $Cu^{II}$-induced synuclein aggregation up to 50%.

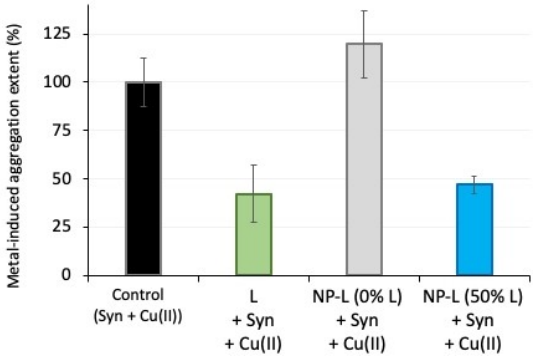


**Figure 8.** Relative metal-induced aggregation extent of Syn-$Cu^{II}$ system (control) alone or co-incubated with L or NPs containing different amounts of PLA-*b*-$PEG_{5k}$-$CH_2CON$–L in the copolymer fraction (0 and 50%). The Syn:Cu:NP molar ratio was 1:3:0.1, and the experimental concentration of Syn was 50 μM.

## Supporting Information Summary

The authors have cited additional references within the Supporting Information.[56–74]

## Acknowledgements

A. M.-C. wants to thank the Generalitat Valenciana and the ESF for the postdoc grant APOSTD/2020/065. This contribution is based upon work from COST Action CA18202, NECTAR—Network for Equilibria and Chemical Thermodynamics Advanced Research, supported by COST (European Cooperation in Science and Technology). CNRS and University Paris-Saclay are also acknowledged for funding. Financial support from the Spanish Ministerio de Ciencia e Innovación (Project PID2019-110751RD–I00) and the Conselleria de Innovación, Universidades, Ciencia y Sociedad Digital of the Generalitat Valenciana (PROMETEO Grant CIPROM/2021/030) is also acknowledged.

## Conflict of Interests

The authors declare no conflict of interest.

## Data Availability Statement

The data that support the findings of this study are available from the corresponding author upon reasonable request.

**Keywords:** Aggregation · Nanozyme · Polymers · Superoxide dismutase activity · α-Synuclein

[1] World Health Organization, *Parkinson Disease: A Public Health Approach. Technical Brief*, ISBN 978-92-4-005098-3, Editor: World Health Organization, © World Health Organization, **2022**, pp. 32.
[2] B. R. Bloem, M. S. Okun, C. Klein, *Lancet* **2021**, *397*, 2284.
[3] E. R. Dorsey, B. R. Bloem, *JAMA Neurol.* **2018**, *75*, 9.
[4] GBD 2016 Neurology Collaborators, Valery L. Feigin, et al., *Lancet Neurol.* **2019**, *18*, 459
[5] B. G. Trist, D. J. Hare, K. L. Double, *Aging Cell* **2019**, *18*, 1.
[6] J. Jankovic, E. K. Tan, *J. Neurol. Neurosurg. Psychiatry* **2020**, *91*, 795.
[7] P. Chopade, N. Chopade, Z. Zhao, S. Mitragotri, R. Liao, V. Chandran Suja, *Bioeng. Transl. Med.* **2023**, *8*, 1.
[8] B. G. Trist, J. B. Hilton, D. J. Hare, P. J. Crouch, K. L. Double, *Angew. Chemie Int. Ed.* **2021**, *60*, 9215.
[9] V. Dias, E. Junn, M. M. Mouradian, *J. Parkinsons. Dis.* **2013**, *3*, 461.
[10] J. Zheng, J. Winderickx, V. Franssens, B. Liu, *Front. Mol. Neurosci.* **2018**, *11*, 1.
[11] T. Jiang, Q. Sun, S. Chen, *Prog. Neurobiol.* **2016**, *147*, 1.
[12] L. Puspita, S. Y. Chung, J. Shim, *Mol. Brain* **2017**, *10*, 53.
[13] A. B. Caballero, P. Gamez, *Angew. Chemie Int. Ed.* **2021**, *60*, 41.
[14] E. Chau, H. Kim, J. Shin, A. Martinez, J. R. Kim, *Biochem. Biophys. Res. Commun.* **2021**, *574*, 85.

[15] E. Lévy, N. El Banna, D. Baïlle, A. Heneman-Masurel, S. Truchet, H. Rezaei, M.-E. Huang, V. Béringue, D. Martin, L. Vernis, *Int. J. Mol. Sci.* **2019**, *20*, 3896.
[16] B. G. Poulson, K. Szczepski, J. I. Lachowicz, L. Jaremko, A.-H. Emwas, M. Jaremko, *RSC Adv.* **2020**, *10*, 215.
[17] Á. Martínez-Camarena, P. A. Sánchez-Murcia, S. Blasco, L. González, E. García-España, *Chem. Commun.* **2020**, *56*, 7511.
[18] D. P. Riley, *Chem. Rev.* **1999**, *99*, 2573.
[19] Á. Martínez-Camarena, A. Liberato, E. Delgado-Pinar, A. G. Algarra, J. Pitarch-Jarque, J. M. Llinares, M. Á. Mañez, A. Domenech-Carbó, *Inorg. Chem.* **2018**, *57*, 10961.
[20] K. N. Green, K. Pota, G. Tircsó, R. A. Gogolák, O. Kinsinger, C. Davda, K. Blain, S. M. Brewer, P. Gonzalez, H. M. Johnston, G. Akkaraju, *Dalt. Trans.* **2019**, *48*, 12430.
[21] C. Policar, J. Bouvet, H. C. Bertrand, N. Delsuc, *Curr. Opin. Chem. Biol.* **2022**, *67*, 102109.
[22] M. Patriarca, V. Daier, G. Camí, N. Pellegri, E. Rivière, C. Hureau, S. Signorella, *Microporous Mesoporous Mater.* **2019**, *279*, 133.
[23] N. Bognanni, F. Bellia, G. Vecchio, *ChemMedChem* **2023**, *18*, e202300035.
[24] M. A. Mekhail, K. J. Smith, D. M. Freire, K. Pota, N. Nguyen, M. E. Burnett, K. N. Green, *Inorg. Chem.* **2023**, *62*, 5415.
[25] Á. Martínez-Camarena, M. Merino, A. V. Sánchez-Sánchez, S. Blasco, J. M. Llinares, J. L. Mullor, E. García-España, *Chem. Commun.* **2022**, *58*, 5021.
[26] Z. Garda, E. Molnár, N. Hamon, J. L. Barriada, D. Esteban-Gómez, B. Váradi, V. Nagy, K. Pota, F. K. Kálmán, I. Tóth, N. Lihi, C. Platas-Iglesias, É. Tóth, R. Tripier, G. Tircsó, *Inorg. Chem.* **2021**, *60*, 1133.
[27] L. Senft, J. L. Moore, A. Franke, K. R. Fisher, A. Scheitler, A. Zahl, R. Puchta, D. Fehn, S. Ison, S. Sader, I. Ivanović-Burmazović, C. R. Goldsmith, *Chem. Sci.* **2021**, *12*, 10483.
[28] M. B. Ward, A. Scheitler, M. Yu, L. Senft, A. S. Zillmann, J. D. Gorden, D. D. Schwartz, I. Ivanović-Burmazović, C. R. Goldsmith, *Nat. Chem.* **2018**, *10*, 1207.
[29] A. Scior, A. Buntru, K. Arnsburg, A. Ast, M. Iburg, K. Juenemann, M. L. Pigazzini, B. Mlody, D. Puchkov, J. Priller, E. E. Wanker, A. Prigione, J. Kirstein, *EMBO J.* **2018**, *37*, 282.
[30] C. D. Kamat, S. Gadal, M. Mhatre, K. S. Williamson, Q. N. Pye, K. Hensley, *J. Alzheimer's Dis.* **2008**, *15*, 473.
[31] Á. Martínez-Camarena, E. Delgado-Pinar, C. Soriano, J. Alarcón, J. M. Llinares, R. Tejero, E. García-España, *Chem. Commun.* **2018**, *54*, 3871.
[32] K. M. Lincoln, P. Gonzalez, T. E. Richardson, D. Julovich, R. Saunders, J. W. Simpkins, K. N. Green, *Chem. Commun.* **2013**, *49*, 2712.
[33] Á. Martínez-Camarena, J. M. Llinares, A. Domenech-Carbó, J. Alarcón, E. García-España, *RSC Adv.* **2019**, *9*, 41549.
[34] C. H. Chung, W. Jung, H. Keum, T. W. Kim, S. Jon, *ACS Nano* **2020**, *14*, 6887.
[35] C. Fasting, C. A. Schalley, M. Weber, O. Seitz, S. Hecht, B. Koksch, J. Dernedde, C. Graf, E. W. Knapp, R. Haag, *Angew. Chemie Int. Ed.* **2012**, *51*, 10472.
[36] J. Pujols, S. Peña-Díaz, D. F. Lázaro, F. Peccati, F. Pinheiro, D. González, A. Carija, S. Navarro, M. Conde-Giménez, J. García, S. Guardiola, E. Giralt, X. Salvatella, J. Sancho, M. Sodupe, T. F. Outeiro, E. Dalfó, S. Ventura, *Proc. Natl. Acad. Sci* **2018**, *115*, 10481.
[37] M. Kurnik, C. Sahin, C. B. Andersen, N. Lorenzen, L. Giehm, H. Mohammad-Beigi, C. M. Jessen, J. S. Pedersen, G. Christiansen, S. V. Petersen, R. Staal, G. Krishnamurthy, K. Pitts, P. H. Reinhart, F. A. A. Mulder, S. Mente, W. D. Hirst, D. E. Otzen, *Cell Chem. Biol.* **2018**, *25*, 1389.
[38] L. Tatenhorst, K. Eckermann, V. Dambeck, L. Fonseca-Ornelas, H. Walle, T. Lopes da Fonseca, J. C. Koch, S. Becker, L. Tönges, M. Bähr, T. F. Outeiro, M. Zweckstetter, P. Lingor, *Acta Neuropathol. Commun.* **2016**, *4*, 39.
[39] M. Perni, C. Galvagnion, A. Maltsev, G. Meisl, M. B. D. Müller, P. K. Challa, J. B. Kirkegaard, P. Flagmeier, S. I. A. Cohen, R. Cascella, S. W. Chen, R. Limbocker, P. Sormanni, G. T. Heller, F. A. Aprile, N. Cremades, C. Cecchi, F. Chiti, E. A. A. Nollen, T. P. J. Knowles, M. Vendruscolo, A. Bax, M. Zasloff, C. M. Dobson, *Proc. Natl. Acad. Sci.* **2017**, *114*, E1009.
[40] K. Ono, M. Tsuji, T. R. Yamasaki, G. M. Pasinetti, *Molecules* **2020**, *25*, 2444.
[41] N. Zhao, X. Yang, H. R. Calvelli, Y. Cao, N. L. Francis, R. A. Chmielowski, L. B. Joseph, Z. P. Pang, K. E. Uhrich, J. Baum, P. V. Moghe, *Front. Bioeng. Biotechnol.* **2020**, *8*, 1.
[42] S. Li, A. Raja, M. Noroozifar, K. Kerman, *ACS Chem. Neurosci.* **2022**, *13*, 1178.
[43] M. Liang, X. Yan, *Acc. Chem. Res.* **2019**, *52*, 2190.
[44] J. Nicolas, S. Mura, D. Brambilla, N. Mackiewicz, P. Couvreur, *Chem. Soc. Rev.* **2013**, *42*, 1147.
[45] D. Brambilla, R. Verpillot, B. Le Droumaguet, J. Nicolas, M. Taverna, J. Kóňa, B. Lettiero, S. H. Hashemi, L. De Kimpe, M. Canovi, M. Gobbi, V. Nicolas, W. Scheper, S. M. Moghimi, I. Tvaroška, P. Couvreur, K. Andrieux, *ACS Nano* **2012**, *6*, 5897.
[46] X. Liu, C. Corciulo, S. Arabagian, A. Ulman, B. N. Cronstein, *Sci. Rep.* **2019**, *9*, 7430.
[47] B. Verdejo, A. Ferrer, S. Blasco, C. E. Castillo, J. González, J. Latorre, M. A. Máñez, M. G. Basallote, C. Soriano, E. García-España, *Inorg. Chem.* **2007**, *46*, 5707.
[48] D. Brambilla, J. Nicolas, B. Le Droumaguet, K. Andrieux, V. Marsaud, P.-O. Couraud, P. Couvreur, *Chem. Commun.* **2010**, *46*, 2602.
[49] E. García-España, M. P. Clares, C. Soriano, S. Blasco, B. Verdejo, J. González, **2012**, ES2355784B1.
[50] H. Ohtsu, Y. Shimazaki, A. Odani, O. Yamauchi, W. Mori, S. Itoh, S. Fukuzumi, *J. Am. Chem. Soc.* **2000**, *122*, 5733.
[51] O. Iranzo, *Bioorg. Chem.* **2011**, *39*, 73.
[52] V. Lanza, F. Bellia, E. Rizzarelli, *Coord. Chem. Rev.* **2018**, *369*, 1.
[53] E. Falcone, I. M. M. Ahmed, V. Oliveri, F. Bellia, B. Vileno, Y. El Khoury, P. Hellwig, P. Faller, G. Vecchio, *Chem. Eur. J.* **2020**, *26*, 1871.
[54] M. Biancalana, S. Koide, *Biochim. Biophys. Acta, Proteins Proteomics* **2010**, *1804*, 1405.
[55] V. Greco, I. Naletova, I. M. M. Ahmed, S. Vaccaro, L. Messina, D. La Mendola, F. Bellia, S. Sciuto, C. Satriano, E. Rizzarelli, *Sci. Rep.* **2020**, *10*, 15998.
[56] E. Falcone, I. M. M. Ahmed, V. Oliveri, F. Bellia, B. Vileno, Y. El Khoury, P. Hellwig, P. Faller, G. Vecchio, *Chem. Eur. J.* **2020**, *26*, 1871.
[57] T. Betancourt, J. D. Byrne, N. Sunaryo, S. W. Crowder, M. Kadapakkam, S. Patel, S. Casciato, L. Brannon-Peppas, *J. Biomed. Mater. Res. Part A* **2009**, *91 A*, 263.
[58] T. Özel, S. White, E. Nguyen, A. Moy, N. Brenes, B. Choi, T. Betancourt, *Lasers Surg. Med.* **2015**, *47*, 579.
[59] C. L. Hamon, C. L. Dorsey, T. Özel, E. M. Barnes, T. W. Hudnall, T. Betancourt, *J. Nanoparticle Res.* **2016**, *18*, 207.
[60] B. Neises, W. Steglich, *Angew. Chemie Int. Ed. English* **1978**, *17*, 522.
[61] G. Hermanson, *Bioconjugate Techniques*, 3rd ed, Elsevier **2013**.
[62] A. Jordan, K. D. Whymark, J. Sydenham, H. F. Sneddon, *Green Chem.* **2021**, *23*, 6405.
[63] M. R. Willcott, *J. Am. Chem. Soc.* **2009**, *131*, 13180.
[64] R. Hidalgo-Álvarez, A. Martín, A. Fernández, D. Bastos, F. Martínez, *Adv. Colloid Interf. Sci.* **1996**, *67*, 1.
[65] L. W. Oberley, D. R. Spitz, *Oxygen Radicals in Biological Systems*, Elsevier **1984**.
[66] L. W. Oberley, D. R. Spitz, *Handbook of Methods of Oxygen Radicals Research* (Ed: R. A. Grenwald), CRC Press, Boca Raton, USA **1986**.
[67] C. Beauchamp, I. Fridovich, *Anal. Biochem.* **1971**, *44*, 276.
[68] J. Y. Zhou, P. Prognon, *J. Pharm. Biomed. Anal.* **2006**, *40*, 1143.
[69] B. H. J. Bielski, H. W. Richter, *J. Am. Chem. Soc.* **1977**, *99*, 3019.
[70] R. F. Pasternack, B. Halliwell, *J. Am. Chem. Soc.* **1979**, *101*, 1026.
[71] S. Durot, C. Policar, F. Cisnetti, F. Lambert, J.-P. Renault, G. Pelosi, G. Blain, H. Korri-Youssoufi, J.-P. Mahy, *Eur. J. Inorg. Chem.* **2005**, *2005*, 3513.
[72] R. Khurana, C. Coleman, C. Ionescu-Zanetti, S. A. Carter, V. Krishna, R. K. Grover, R. Roy, S. Singh, *J. Struct. Biol.* **2005**, *151*, 229.
[73] S.-T. Sun, H. Wang, D. Huang, Y.-L. Ding, Y. Zhang, D.-P. Song, K.-Y. Zhang, L. Pan, Y.-S. Li, *Chin. J. Polym. Sci.* **2020**, *38*, 1335.
[74] I. Z. Kozma, P. Krok, E. Riedle, *J. Opt. Soc. Am. B* **2005**, *22*, 1479.

Manuscript received: April 3, 2024
Accepted manuscript online: April 30, 2024
Version of record online: May 22, 2024